doi:10.1246/cl.2012.546
546 Published on the web April 28, 2012

Room-temperature Fast Synthesis of Composition-adjustable Pt–Pd Alloy Sub-10-nm Nanoparticle Networks with Improved Electrocatalytic Activities

Shuangxia Hou, You Xu, Yang Liu,* Rui Xu, and Bin Zhang*
Department of Chemistry, School of Science, Tianjin University, Tianjin 300072, P. R. China

(Received February 13, 2012; CL-120116; E-mail: bzhang@tju.edu.cn)

Pt–Pd alloy nanoparticle networks (Pt–Pd NN) with adjustable composition have been fast synthesized through a one-step room-temperature coreduction method in a water/ethylene glycol (EG) system. It was found that the Pt–Pd NN exhibited enhanced electrocatalytic activity toward ethanol oxidation reaction (EOR) compared with Pt nanoparticle networks (Pt NN) and commercially available Pt black.

Over the past few decades, Pt-based nanomaterials,[1,2] especially Pt-based bimetallic alloy nanomaterials have attracted extensive interest because of their higher catalytic properties relative to single composition, such as selectivity, activity, and stability.[3–5] The catalytic properties of bimetallic alloy nanomaterials are highly dependent on their chemical composition, size, and shapes.[6–10] Owing to their superior catalytic properties, Pt–Pd alloy nanostructures are among the most interesting bimetallic nanomaterials.[11–15] Various Pt–Pd alloy nanostructures can be prepared by either a seed-mediated growth method or successive coreduction of Pt and Pd species. For instance, Yang et al. prepared binary Pt/Pd nanoparticles by growth of Pd on the cubic Pt seeds in aqueous tetradecyltrimethylammonium bromide (TTAB) solution in the presence of $NaBH_4$.[11] Also, Zheng and co-workers successfully synthesized hollow Pt/Pd alloy nanocubes by heating the precursor solution at 150 °C.[12] Among various Pt–Pd nanostructures, porous or network-like Pt–Pd alloy nanostructures with sponge shapes represent a very interesting new type of structure, which may be highly exciting electrocatalysts with high activity. In comparison with other solid nanostructures, porous or network-structured Pt–Pd alloy electrocatalysts could not only provide larger electrochemically active surface area and more Pt active sites, but also effectively prevent the agglomeration of catalysts.

Recently, we have reported a one-step high-yield strategy to synthesize 3D porous network-structured noble metals and alloys.[16] However, this synthesis strategy is time-consuming and requires high reaction temperature. Additionally, the size of obtained building blocks of the network was over 20 nm, which may result in the decrease of the specific surface area and lower the utilization of the electrocatalysts. Very recently, we also developed a room-temperature soft-template-assisted water–chloroform approach to synthesize Pt_3Ni networks.[17] Although the two-phase method is very efficient in producing porous network, organic solvent is necessary for producing two-phase interface. However, developing a facile, organic-solvent-free, environmental friendly, and room-temperature approach to fabricate metal alloy nanoparticle network structures with sub-10 nm nanoparticles remains challenging.

Herein, we report a simple, inexpensive, sodium borohydride reduction process in a water/ethylene glycol (EG) system to prepare Pt–Pd alloy nanoparticle networks (Pt–Pd NN) at room temperature. The composition of the Pt–Pd NN can be modulated by changing the molar ratio of metal salts. It was found that the as-prepared Pt–Pd NN exhibited reinforced electrocatalytic activity toward ethanol oxidation reaction (EOR) over Pt nanoparticle networks (Pt NN) and commercially available Pt black.

An aqueous solution of $H_2[PtCl_6]$ (20 mmol L^{-1}) and $H_2[PdCl_4]$ (20 mmol L^{-1}) was prepared with Milli-Q deionized water. For the synthesis of $Pt_{0.5}Pd_{0.5}$ NN, 15 mL of Milli-Q deionized water and 30 mL of EG were injected in a 100-mL three-neck flask under magnetic stirring at room temperature. After that, an aqueous solution of 2.5 mL of $H_2[PtCl_6]$ and that of 2.5 mL of $H_2[PdCl_4]$ were put into the above mixed solution. After stirring for 0.5 h, 0.2 g of $NaBH_4$ dissolved in 5 mL of water was added into the flask under constant stirring. The solution quickly turned into a dark color in 1 min, showing the formation of nanoparticle networks. The as-synthesized samples were centrifuged and washed three times with distilled water and then absolute ethanol. For the synthesis of Pt NN, the experimental parameters are the same as for the preparation of Pt–Pd NN except that the mixed metal precursors are replaced by $H_2[PtCl_6]$ (5 mL).

The SEM images and energy-dispersive X-ray spectroscopic (EDX) analysis data were obtained on a Hitachi S-4800 scanning electron microscope equipped with the Thermo Scientific energy-dispersion X-ray fluorescence analyzer. Transmission electron microscopy (TEM) and high-resolution TEM (HRTEM) were carried out using a JEOL-2100F system. X-ray diffraction (XRD) patterns of the samples were recorded on a Bruker D8 focus diffraction system using a Cu Kα radiation ($\lambda = 0.154178$ nm). X-ray photoelectron spectroscopy (XPS) analysis was performed on a PHII600 spectrometer (PE Co., U.K.) using Mg Kα/Al Kα radiation.

All electrochemical measurements were performed in a conventional three-compartment glass cell by using an electrochemical workstation (CHI 660, CH Instruments, Austin, TX). In a typical preparing process of working electrode, 2 mg of catalyst was dispersed in 1 mL of a mixture solvent (the volume ratio of H_2O:5% Nafion is 250:1), and the mixture was sonicated for 5 min to get a dispersed suspension. Then 5 μL of the suspension was dropped onto the working electrode and dried in flowing argon. A Pt-wire and a saturated calomel electrode (SCE) were used as counter electrode and reference electrode, respectively. All potentials were recorded in reference to SCE. All experiments were performed at room temperature. The working electrode was cleaned in 0.1 M H_2SO_4 by scanning the applied potential between −0.3 and +1.25 V at a scan rate of 100 mV s^{-1} for 25 cycles before every measurement.

The morphology and structure of the as-prepared Pt–Pd nanostructures was first characterized by using SEM and TEM.

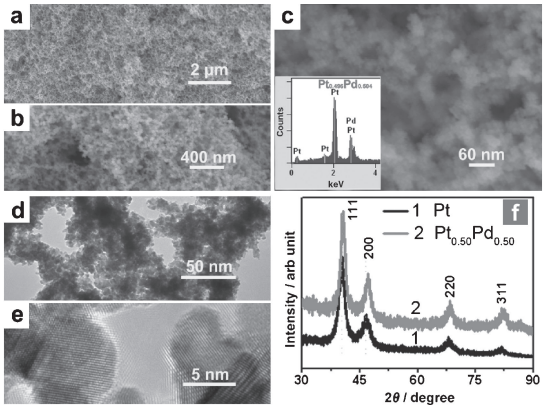

Figure 1. Typical SEM images (a–c), EDX (the inset in Figure 1c), TEM image (d), and HRTEM image (e) of the as-prepared $Pt_{0.5}Pd_{0.5}$ NN. XRD patterns (f) of the as-prepared porous $Pt_{0.5}Pd_{0.5}$ and Pt NN.

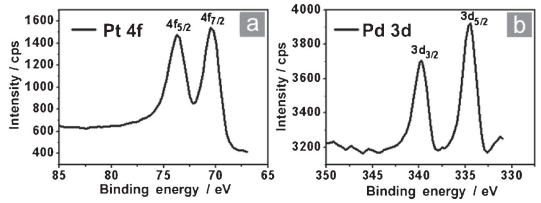

Figure 2. XPS spectra of the as-prepared $Pt_{0.5}Pd_{0.5}$ NN (a, b).

Figures 1a–1c show the typical SEM images of the sample. It can be seen from Figures 1a and 1b that the sample with a sponge-like network structure was prepared on a large scale. The high-magnification SEM image (Figure 1c) further confirms this network-like feature which composed of many nanoparticle-based building blocks. The structural features of the building blocks for the network were further investigated by the TEM and HRTEM images, as shown in Figures 1d and 1e. It is clearly seen that the building blocks were irregular nanoparticles with an average diameter of sub-10 nm. The phase analysis of the as-obtained NN was examined by XRD. Figure 1f shows the XRD patterns of the Pt–Pd and Pt NN. In comparison to pure Pt NN, it was found that corresponding diffraction peaks of Pt–Pd NN shift to the higher 2θ degree, suggesting that the as-obtained Pt–Pd NN are Pt–Pd alloy rather than the mixture of Pt and Pd. The EDX analysis of Pt–Pd NN (the inset of Figure 1c) shows that the nanoparticle network-like samples are composed of Pt and Pd with a atomic ratio of ca. 1:1, which is consistent with the XPS data and in agreement with the adding ratio of the metal precursors.

Figures 2a and 2b show the characteristic spectra of Pt 4f and Pd 3d. Two strong peaks at around 70.43 and 73.69 eV displayed in Figure 2a can be attributed to Pt $4f_{7/2}$ and Pt $4f_{5/2}$. The binding energies of 334.51 and 339.77 eV correspond to Pd $3d_{5/2}$ and Pd $3d_{3/2}$, as seen in Figure 2b.

By varying the relative ratio of $H_2[PtCl_6]$ and $H_2[PdCl_4]$, the composition of Pt in Pt–Pd NN can be modulated, but the size of building blocks in NN does not experience an obvious change, as shown in Figure 3 and Figure S1.[26]

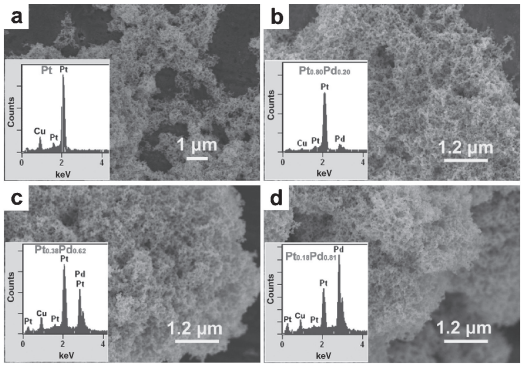

Figure 3. SEM images (a–d) and the corresponding EDX results (the inset of a–d): (a) Pt NN, (b) $Pt_{0.80}Pd_{0.20}$ NN, (c) $Pt_{0.38}Pd_{0.62}$ NN, and (d) $Pt_{0.18}Pd_{0.82}$ NN.

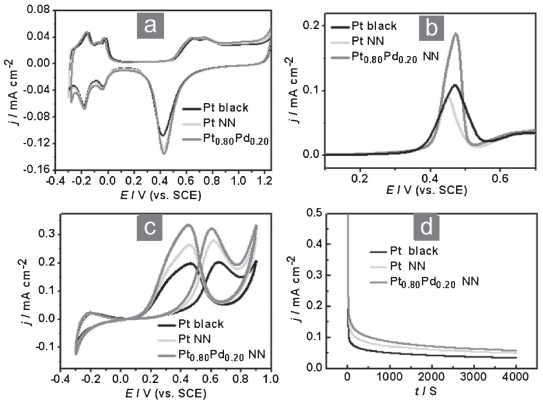

Figure 4. Pt black, Pt, and $Pt_{0.80}Pd_{0.20}$ NN: (a) CVs, (b) typical CO stripping voltammograms, (c) CVs of EOR, and (d) chronoamperometric curves.

As for the formation mechanism, it is thought that enough amount of $NaBH_4$ solution was added to mixed metal precursors to form lots of small metal nuclei,[18] which is easy to fuse to form chain-networks of alloy due to the high surface energy of small nuclei in the absence of any surfactants or polymers. These chain-like networks can be used for further growth of final Pt–Pd networks via Ostwald ripening.

To further probe the intrinsic properties of the as-prepared Pt–Pd alloy, the electrocatalytic activities of $Pt_{0.80}Pd_{0.20}$ NN were tested and compared with those of commercially available Pt black (Aldrich) and Pt NN obtained using our synthesis method. Figure 4a shows the CV curves of these three catalysts recorded in a 0.1 M H_2SO_4 solution at a scan rate of 50 mV s^{-1}. It is clearly seen that Pt–Pd NN and Pt NN exhibit the similar CV behavior to that of Pt black. It is found that the well-defined hydrogen adsorption/desorption peaks appeared for the three catalysts. Figure 4b shows typical CO stripping voltammograms for Pt black, Pt NN, and $Pt_{0.80}Pd_{0.20}$ NN. The potentials of their CO stripping peaks are 0.468, 0.449, and 0.472 V, respectively. It is deduced that with the increase of the amount of Pd, the potential of the CO stripping peaks shifts toward more positive potentials. We found that the CO stripping peak of pure Pd NN is 0.681 V (not shown here). This result seems to be related to

the adjustment of the surface electronic structure of Pt–Pd NN.[19] The electrochemically active surface areas (ECSA) of Pt catalyst could be determined by integrating the hydrogen adsorption/desorption areas of the CV curve (210 $\mu C\,cm^{-2}_{Pt}$). Because Pd metal absorbs hydrogen species, the CO stripping peak is employed to calculate the ECSA of the Pd-containing Pt–Pd catalysts surfaces according to a reported method.[19]

Figure 4c shows the representative voltammograms of EOR on Pt black, Pt NN, and $Pt_{0.80}Pd_{0.20}$ NN obtained in 0.1 M ethanol and 0.1 M H_2SO_4 at a scan rate of 50 mV s^{-1}. It can be easily observed that the voltammograms on these three catalysts display a similar profile. Generally, at potential below 0.2 V, the oxidation current is very low in all three voltammograms because the active sites are poisoned by CO_{ads}, an intermediate from dehydrogenation of ethanol. At more positive potential, the oxidation current increases rapidly. The peak potential of the ethanol oxidation on $Pt_{0.80}Pd_{0.20}$ is 0.600 V in the positive scan, which is about 16 mV lower than that on Pt NN (0.616 V) and 50 mV lower than that on Pt black (0.650 V). The corresponding current density on $Pt_{0.80}Pd_{0.20}$ NN is 0.322 mA cm^{-2} in the positive scan, which is 1.15 times and 1.69 times larger than those on Pt NN (0.280 mA cm^{-2}) and Pt black (0.202 mA cm^{-2}), respectively. In the negative potential scan, the current peak appears at 0.449 V, which also shifts negatively relative to those on Pt NN and Pt black. Also, the current density on $Pt_{0.80}Pd_{0.20}$ NN in the reversed potential scan is significantly larger than those on other two catalysts. The negatively shifted peak potentials and increased peak current densities indicated that $Pt_{0.80}Pd_{0.20}$ NN exhibited remarkable enhanced electrocatalytic activities toward EOR over Pt NN and Pt black. The catalytic enhancement may be attributed to incorporation of Pd, which is favorable for reducing the electronic binding energy in Pt and facilitating the C–H cleavage reaction in ethanol decomposition.[20–25]

Chronoamperometry (CA) tests of Pt black, Pt NN, and $Pt_{0.80}Pd_{0.20}$ NN were conducted for 4000 s to examine the extended stability in EOR, as presented in Figure 4d. At a potential of 0.6 V versus SCE, $Pt_{0.80}Pd_{0.20}$ NN catalyst exhibits the highest current density. It shows that from 0 to about 2000 s, the current density at Pt black decreases from 0.110 mA cm^{-2} to 0.050 mA cm^{-2}, the decrease of the current density is likely due to the surface poisoning from CO_{ads}, which is generated from EOR. However, the current density at Pt NN decreases from 0.136 mA cm^{-2} to 0.073 mA cm^{-2}, and $Pt_{0.80}Pd_{0.20}$ NN decreases from 0.169 mA cm^{-2} to 0.090 mA cm^{-2}. Therefore, the CA data studied here confirm that proper Pd-containing catalyst exhibits higher activity and better long-term stability, which may be important for practical applications.

In summary, Pt–Pd NN has been successfully synthesized through a one-step coreduction method in a water/EG system at room temperature. The composition of the Pt–Pd NN could be adjusted by controlling Pt:Pd ratio of the precursors. Electrochemical measurements show that the composition of the NN determines their activities and stability for the EOR. The $Pt_{0.80}Pd_{0.20}$ NN had much higher electrocatalytic activity toward EOR over Pt NN and commercially available Pt black. We expect that this charge-controlled synthesis method will in the future trigger the facile creation of novel NN structures with designed compositions and desired properties.

This work was financially supported by the National Natural Science Foundation of China (Nos. 20901057 and 11074185), the Tianjin Natural Science Foundation (No. 10JCYBJC01800), State Key Laboratory of Crystal Materials at Shandong University (No. KF0910), Innovation Foundation of Tianjin University, and the Scientific Research Foundation for the Returned Overseas Chinese Scholars, State Education Ministry.

References and Notes

1 J. Yuan, D. Han, Y. Zhang, Y. Shen, Z. Wang, Q. Zhang, L. Niu, *J. Electroanal. Chem.* **2007**, *599*, 127.
2 J. Yuan, Z. Wang, Y. Zhang, Y. Shen, D. Han, Q. Zhang, X. Xu, L. Niu, *Thin Solid Films* **2008**, *516*, 6531.
3 N. Toshima, H. Naohara, T. Yoshimoto, Y. Okamoto, *Chem. Lett.* **2011**, *40*, 1095.
4 S. Takenaka, Y. Orita, T. Arike, H. Matsune, E. Tanabe, M. Kishida, *Chem. Lett.* **2007**, *36*, 1250.
5 Y.-F. Zhou, J. Wei, G.-Y. Fan, H.-y. Fu, R.-X. Li, H. Chen, X.-J. Li, *Chem. Lett.* **2009**, *38*, 1034.
6 M. Murata, Y. Tanaka, T. Mizugaki, K. Ebitani, K. Kaneda, *Chem. Lett.* **2005**, *34*, 272.
7 A. Chen, P. Holt-Hindle, *Chem. Rev.* **2010**, *110*, 3767.
8 Z. Peng, H. Yang, *Nano Today* **2009**, *4*, 143.
9 W. Chen, S. Chen, *J. Mater. Chem.* **2011**, *21*, 9169.
10 Y. S. Kim, S. H. Nam, H.-S. Shim, H.-J. Ahn, M. Anand, W. B. Kim, *Electrochem. Commun.* **2008**, *10*, 1016.
11 H. Lee, S. E. Habas, G. A. Somorjai, P. Yang, *J. Am. Chem. Soc.* **2008**, *130*, 5406.
12 X. Huang, H. Zhang, C. Guo, Z. Zhou, N. Zheng, *Angew. Chem., Int. Ed.* **2009**, *48*, 4808.
13 Q. Yuan, Z. Zhou, J. Zhuang, X. Wang, *Chem. Commun.* **2010**, *46*, 1491.
14 L. Zhang, J. Zhang, Z. Jiang, S. Xie, M. Jin, X. Han, Q. Kuang, Z. Xie, L. Zheng, *J. Mater. Chem.* **2011**, *21*, 9620.
15 B. Lim, J. Wang, P. H. C. Camargo, C. M. Cobley, M. J. Kim, Y. Xia, *Angew. Chem., Int. Ed.* **2009**, *48*, 6304.
16 J. Cui, H. Zhang, Y. Yu, Y. Liu, Y. Tian, B. Zhang, *J. Mater. Chem.* **2012**, *22*, 349.
17 Y. Xu, S. Hou, Y. Liu, Y. Zhang, H. Wang, B. Zhang, *Chem. Commun.* **2012**, *48*, 2665.
18 K. S. Krishna, C. S. S. Sandeep, R. Philip, M. Eswaramoorthy, *ACS Nano* **2010**, *4*, 2681.
19 T. Vidaković, M. Christov, K. Sundmacher, *Electrochim. Acta* **2007**, *52*, 5606.
20 H. Li, G. Sun, N. Li, S. Sun, D. Su, Q. Xin, *J. Phys. Chem. C* **2007**, *111*, 5605.
21 L. Wang, Y. Nemoto, Y. Yamauchi, *J. Am. Chem. Soc.* **2011**, *133*, 9674.
22 A.-X. Yin, X.-Q. Min, Y.-W. Zhang, C.-H. Yan, *J. Am. Chem. Soc.* **2011**, *133*, 3816.
23 Y. W. Lee, M. Kim, Y. Kim, S. W. Kang, J.-H. Lee, S. W. Han, *J. Phys. Chem. C* **2010**, *114*, 7689.
24 C. Xu, A. Liu, H. Qiu, Y. Liu, *Electrochem. Commun.* **2011**, *13*, 766.
25 H. Yang, J. Zhang, K. Sun, S. Zou, J. Fang, *Angew. Chem., Int. Ed.* **2010**, *49*, 6848.
26 Supporting Information is also available electronically on the CSJ-Journal Web site, http://www.csj.jp/journals/chem-lett/index.html.

